NIH Public Access
Author Manuscript
Biomech Model Mechanobiol. Author manuscript; available in PMC 2014 August 01.

Published in final edited form as:
Biomech Model Mechanobiol. 2013 August ; 12(4): 735–745. doi:10.1007/s10237-012-0437-0.

Atrial Fibrillation Pacing Decreases Intravascular Shear Stress in a New Zealand White Rabbit Model: Implications in Endothelial Function

Nelson Jen[#], **Fei Yu**[#], **Juhyun Lee**, **Steve Wasmund**[*], **Xiaohu Dai**, **Christina Chen**, **Pai Chawareeyawong**, **Yongmo Yang**[**], **Rongsong Li**, **Mohamed H. Hamdan**[*], and **Tzung Hsiai**
Department of Biomedical Engineering and Cardiovascular Medicine, University of Southern California School of Engineering and Medicine, Los Angeles, CA 90089

[*]Division of Cardiovascular Medicine, University of Wisconsin School of Medicine and Public Health, Madison, WI 53792

[**]Department of Electrical Engineering, Arizona State University, Tempe, AZ 85281

Abstract

Atrial fibrillation (AF) is characterized by multiple rapid and irregular atrial depolarization leading to rapid ventricular responses exceeding 100 beats per minute (bpm). We hypothesized that rapid and irregular pacing reduced intravascular shear stress (ISS) with implication to modulating endothelial responses. To simulate AF, we paced the left atrial appendage of New Zealand White (NZW) rabbits (n=4) at rapid and irregular intervals. Surface electrical cardiograms (ECG) were recorded for atrial and ventricular rhythm, and intravascular convective heat transfer was measured by micro thermal sensors, from which ISS was inferred. Rapid and irregular pacing decreased arterial systolic and diastolic pressures (baseline: 99/75 mmHg; rapid regular pacing: 92/73; rapid irregular pacing: 90/68; $P < 0.001$, n=4), temporal gradients ($\partial\tau/\partial t$ from 1275 ± 80 to 1056 ± 180 dyne/cm^2·s), and reduced ISS (from baseline at 32.0 ± 2.4 to 22.7 ± 3.5 dyne/cm^2). Computational fluid dynamics (CFD) code demonstrated that experimentally inferred ISS provided a close approximation to the computed wall shear stress (WSS) at a given catheter to vessel diameter ratio, shear stress range, and catheter position. In an i*n vitro* flow system in which time-averaged shear stress was maintained at τ_{avg}=23 ±4 dyn·cm^{-2}·s^{-1}, we further demonstrated that rapid pulse rates at 150 bpm down-regulated endothelial nitric oxide (NO), promoted superoxide ($O_2^{\cdot-}$) production, and increased monocyte binding to endothelial cells. These findings suggest that rapid pacing reduces ISS and $\partial\tau/\partial t$, and rapid pulse rates modulate endothelial responses.

Keywords

Atrial Fibrillation; Shear Stress; Endothelial Cells; NO; ROS; Monocyte Binding

Introduction

Cardiac arrhythmia is a leading cause of syncope and sudden cardiac death in the United State (Wann et al. 2011; Zipes et al. 2006; Skalidis et al. 2008; Deedwania and Lardizabal

Corresponding Author: zung K. Hsiai, M.D., Ph.D., Division of Cardiovascular Medicine and Biomedical Engineering, University of Southern California, Los Angeles, CA 90089, hsiai@usc.edu, Telephone: (213)740-7236, Fax: (213) 740-0343.
[#]Both authors contributed equally.

The authors have no conflict of interest.

NIH-PA Author Manuscript
NIH-PA Author Manuscript
NIH-PA Author Manuscript

NIH-PA Author Manuscript

NIH-PA Author Manuscript

NIH-PA Author Manuscript

2010; Nattel 2002). Atrial fibrillation (AF) is the most common type of cardiac arrhythmia, affecting up to 5 million people in the United states and 5% of the population over 65 years old (Go et al. 2001; Nattel 2011; Fuster et al. 2006). While the effects of AF-mediated atrial remodeling have been widely characterized (Fuster et al. 2006; Guazzi and Arena 2009), the hemodynamic effects of AF on endothelial function has remained poorly understood.

Mounting evidence suggests that AF is implicated in increased serum oxidative stress markers and impaired acetylcholine-mediated vasodilation (Ehrlich et al. 2011; Matsue et al. 2011; Goette et al. 2012; Raviele and Ronco 2010). AF promotes rapid and irregular atrial contraction rates exceeding 400–600 times per minute (bpm) (Nattel 2002), resulting in rapid and irregular ventricular contraction rates above 100 bpm (Haissaguerre et al. 1998), and leading to a decrease in both atrial pressure and cardiac output (Kern et al. 2009; Clark et al. 1997). While a plethora of literature supports the mechanisms linking wall shear stress with regulation of endothelial function (Li et al. 2005; Papafaklis et al. 2010), there is a paucity of data to support AF-mediated changes in hemodynamics on endothelial responses.

In this context, we sought to determine whether AF-mediated changes in temporal gradients ($\partial\tau/\partial t$) and intravascular shear stress (ISS) modulated endothelial responses. Microelectromechanical systems (MEMS) thermal sensors have allowed for measurement of convective heat transfer in the aorta of New Zealand White (NZW) rabbits, from which intravascular shear stress (ISS) was inferred as an approximation to wall shear stress (Hwang et al. 2003; Yu et al. 2008; Ai et al. 2010; Ai et al. 2009a; Ai et al. 2009b; Yu et al. 2011). Surface electrical cardiogram (ECG) recordings were synchronized with ISS in the thoracic aorta in response to rapid and irregular atrial pacing. In an i*n vitro* flow system in which the time-averaged shear stress was maintained at a constant value, we further assessed the effects of rapid pulse rates on the production of endothelial nitric oxide (NO), reactive oxygen species (ROS), and on monocyte binding to human aortic endothelial cells (HAEC). Our findings suggest that rapid atrial pacing reduces ISS and $\partial\tau/\partial t$, and rapid pulse rate is implicated in modulating endothelial function.

Materials and Methods

Catheter-Based Flexible MEMS Sensor to Measure Intravascular Convective Heat Transfer

The sensor was fabricated using surface micromachining with biocompatible materials including Parylene C, Ti, and Pt as previously described (Yu et al. 2008) (Supplementary Figure 1). Based on the heat transfer principle, the output voltage of the MEMS sensors under the constant current circuits was sensitive to the fluctuations of ambient temperature. The temperature overheat ratio (α_T) is expressed as temperature variations of the sensor over the ambient temperature (T_0):

$$\alpha_T = \frac{T - T_0}{T_0}, \quad (1)$$

where T denotes the temperature of the sensor. The relation between resistance and temperature overheat ratios is expressed as:

$$\alpha_R = \frac{R - R_0}{R} = \alpha\ T - T_0 \quad (2)$$

where α is the Temperature Coefficient of Resistance (*TCR*). The operating resistance of the sensing element was approximately 1.189 kΩ at 37.8°C with a temperature overheat ratio (α_T) of 0.046 and a TCR (α) of 0.84×10^{-3}/°C (Supplementary Figure 2a). The sensor provided a maximum frequency response at 5 kHz accompanied by a gain of 8.72

NIH-PA Author Manuscript

NIH-PA Author Manuscript

NIH-PA Author Manuscript

(Supplementary Figure 2b). Calibration was performed in a platinum-cured silicone tube for individual sensors to establish a relationship between heat exchange (from the heated sensing element to the blood flow) and shear stress over a range of steady flow rates (Qn). The theoretical shear stress value corresponding to each flow rate was calculated as:

$$\tau_w = \frac{4Q_n\mu}{\pi r^3} \quad (3)$$

where τ_w is the wall shear stress, μ is the blood viscosity, and r is the radius of the circular tube. The viscosity of the blood as a function of flow rate was measured using a viscometer (Brookfield Engineering, Newhall, CA). The calibrated sensors were then deployed into the NZW rabbit's aorta for convective heat transfer on the MEMS thermal sensors, from which intravascular shear stress (ISS) was inferred as previously described (Hsiai et al. 2004; Ai et al. 2010):

$$\tau_w^{1/3} \propto Q_{conv} \cong \frac{V_0^2}{R_s}, \quad (4)$$

where Q_{conv} denotes the convective heat transfer, V the changes in voltage to the MEMS thermal sensors as flow past the resistively heated sensor, and R the resistors of the sensor.

Assessment of Intravascular Shear Stress

In light of experimental constraints to directly measure wall shear stress in an *in vivo* model, we acquired ISS to approximate wall shear stress in NZW rabbit aortas (Ai et al. 2009b). Flexible MEMS sensors deployment into rabbit aortas was performed in compliance with the Institutional Animal Care and Use Committee in the Heart Institute of the Good Samaritan Hospital (Los Angeles, CA), which is accredited by the American Association for Assessment and Accreditation for Laboratory Animal Care (AAALAC). Four male NZW rabbits (ten weeks old, mean body weight 2442 ± 210 g) were acquired from a local breeder (Irish Farms, Norco, CA) and maintained in the Good Samaritan Hospital Vivarium. After a seven-day quarantine period, the rabbits were anesthetized for percutaneous access, and anesthesia was induced through an intramuscular injection of 50 mg/kg ketamine (JHP Pharmaceuticals, LLC) combined with 10 mg/kg xylazine (IVX Animal Health, Inc.). A 23-gauge hypodermic needle and 26-gauge guide wire were introduced via cut-down of the left femoral artery. A rabbit femoral catheter (0.023 in ID ×0.038 in OD) was passed through the left femoral artery. The circulatory system of the individual animals was anticoagulated with heparin (100 units/kg) prior to the sensor deployment, and catheters and needles were rinsed with heparin at 1000 units/mL prior to the procedures.

An ultrasound transducer (Philips SONOS 5500 at 12 MHz) was positioned over the abdomen to interrogate arterial blood flow. Periodic blood pressure measurements were recorded with an automated tail cuff (IITC/Life Science Instruments). Using the fluoroscope in the animal angiographic laboratory (Phillips BV-22HQ C-arm), we were able to visualize and steer the catheter-based MEMS sensors (Fig. 1a). Contrast dye was injected to delineate the position of the MEMS sensors in relation to the inner aortic diameter. The voltage recordings were synchronized with the rabbit's cardiac cycle via ECG (The ECGenie, Mouse Specifics).

Data Acquisition

The constant temperature circuit was used for real-time voltage signal acquisition in the aorta (Hsiai et al. 2004). When the current passed through the sensor, sensing element was heated up at an overheat ratio of ~3%. The voltage across the sensing element was

NIH-PA Author Manuscript

NIH-PA Author Manuscript

NIH-PA Author Manuscript

monitored by a LabVIEW-based data acquisition system, which included a data acquisition board (USB-6216 DAQ device, National Instruments, Austin, TX) and a laptop computer (ThinkPad T61, Lenovo) loaded with LabVIEW. The acquisition was sampled at 1000 Hz. Wavelet decomposition and low-pass filters were applied to remove background noise, resulting in a signal-to-noise ratio of 4.8 as previously described (Sun et al. 2009).

Rapid Atrial Fibrillation Pacing

Rapid atrial fibrillation (AF) was performed via a standard pacemaker lead (St. Jude Medical, Minneapolis, MN, USA) that was advanced through the jugular vein into the right atrium. The lead was connected directly to a Grass SD9 stimulator (Grass Technologies, West Warwick, RI, USA). The stimulator was triggered using a custom software program (LabVIEW, National Instruments, Austin, TX). The pacing protocols were as follows: 1) baseline sinus rhythm at 121.8 ± 1.6, 2) rapid regular and tachycardia atrial pacing at 168.3±0.5, and 3) rapid irregular pacing at 167.1 ± 57.4 (Table 1).

ECG Recordings and Signal Processing

Two 29-gauge stainless steel micro-electrodes (AD Instrument, Colorado Springs, CO) were positioned at 90° to the animal's ventral epidermis. The recording electrode was positioned directly above the ventricle while the reference electrode was positioned distal to the heart. Both electrodes were secured onto the skin to approximately 1 mm in depth. The ECG signals were amplified by 1,000-fold (A-M 1700 Differential Amplifier, A-M Systems Inc., Carlsborg, WA) and band-pass filtered between 0.1 and 500 Hz as well as at 60 Hz (notch) (Sun et al. 2009). The signals were acquired and digitized at a sampling rate of 1000 Hz (National Instruments USB-6216 DAQ device, and LabVIEW 8.2). To enhance signal-to-noise ratios (SNR), we digitally processed the signals using the wavelet transform and thresholding MATLAB algorithm (MATLAB 7.1 Mathworks Inc, Natick, MA) developed in our laboratory (Yu et al. 2010). The parameters used in the algorithm allowed for systematic recordings for QRS and QTc intervals regardless of electrode placements or the cardiac vector orientations.

Computational Fluid Dynamics (CFD) Simulation

CFD code was developed to compare between analytical and experimental data. Three-dimensional modeling of healthy rabbit aortic geometries (aortic arch, thoracic, abdominal, renal aorta) was reconstructed by SolidWorks (Concord, Massachusetts, USA). To exclude contributions from lumen elasticity, the aorta was assumed to be a rigid tube. Aorta diameters were taken from angiography. The inlet pulsatile blood velocity profiles were obtained from the pulsed-wave Doppler velocity measurements. The velocity values were filtered by a low-pass filter using MATLAB (Natick, MA, USA). To compensate for the model's flat velocity inlet boundary layer, we allowed the fluid to flow along the rigid tube for 20cm to develop fully parabolic flow before the flow stream passes down to the sensor. The outlet boundary condition was determined from the mean arterial pressure and defined as 80 mmHg. Geometries were meshed by 9424 fluid/12484 partial hexahedron cells after defining the inlet and outlet boundary conditions. Meshed models were solved by SolidWorks Flow simulation until it met the defining time which is 2 seconds, with a time step size of 0.005s. SolidWorks Flow simulation automatically setup to meet the convergence condition with changing iterating numbers. The governing equations were solved by assuming laminar, incompressible, and unsteady flow under the non-slip condition.

NIH-PA Author Manuscript

NIH-PA Author Manuscript

NIH-PA Author Manuscript

A Flow System to Assess Cultured Endothelial Responses to Rapid Pulse Rates

A train of pulsatile shear stress (PSS: unidirectional flow) was generated to deliver distinct pulse rates (50 bpm, 100 bpm vs. 150 bpm), slew rates ($\partial\tau/\partial t$ = 31, 57, vs. 89 dyne·cm^{-2}·sec^{-1}), and minimum versus maximal shear stress (12 vs. 36 dyne·cm^{-2}) at a constant time-averaged shear stress (τ_{avg}=23 ±4 dyn·cm^{-2}·s^{-1}) (Supplemental Figure 3). Oscillatory shear stress (OSS at 0.1 ± 3.0 dyne·cm^{-2}) was also generated to compare with PSS.

Human aortic endothelial cells (HAEC) (Cell Applications, San Diego, CA) were cultured on gelatin coated dish in endothelial growth medium (Cell Applications) supplemented with 5 % heat-inactivated fetal bovine serum (FBS, GIBCO, Carlsbad, CA) at 37 °C in a 5 % CO_2 atmosphere. The cells were exposed to five flow conditions for 4 hours: (1) control at static conditions as a reference point, (2) PSS at 50 bpm, (3) PSS at 100 bpm, (3) PSS at 150 bpm, and (5) OSS at 60 bpm (Supplementary Figure 3). Subsequently, the cells were used to assess NO production and monocyte binding assay.

Analysis of NO Production: Nitrite (NO_2^-) and Nitrate (NO_3^-)

Quantitative measurements of NO_2^- and NO_3^- were performed as an index of global nitric oxide ($^{\cdot}NO$) production following methods described previously (Hwang et al. 2006). $^{\cdot}NO$ is metabolized or decomposed via various reactions to the metabolites as NO_2^- and NO_3^-, which serve as useful measurements of overall $^{\cdot}NO$ production and metabolism (Pietraforte et al. 2004).

Measurement of Reactive Oxygen Species (ROS)

The intracellular superoxide ($O_2^{\cdot-}$) production was measured using dihydroethidium (DHE). HAEC were exposed to PSS at 50, 100, 150 bpm, and OSS at 1 Hz for 4 hour, followed by incubation with DHE (5 μM). Images were acquired from three chosen fields (Nikon Inverted Epifluorescence Microscope and a ProgRes C3 digital microscope camera, Japan). Image intensities were quantified by using a custom Matlab script.

Monocyte Binding Assay

THP-1 cells, grown in suspension, were centrifuged, rinsed with phosphate-buffered saline (PBS) twice, and labeled with 1.0 μM Calcein AM (Invitrogen). Following shear stress exposures as described above, HAEC were incubated with Calcein-labeled THP-1 cells for 30 minutes in a humidified incubator with 5% CO^2 at 37°C. Unbound THP-1 cells were washed away three times with PBS. 1 ml of PBS/2%PFA was added and incubated for 30 minutes at room temperature. The cells were rinsed with PBS and 1 ml of PBS was added onto each slide). THP-1 cells attached to endothelial cells were counted under fluorescence microscope. Bound THP-1 cells were counted in five fields for each slide, averaged, and normalized to static control.

Statistical analyses

Data were expressed as mean ± SD. For comparisons between two groups, student t-test was used for significance analysis. For comparisons among multiple values one-way analysis of variance (ANOVA) was used. A p value < 0.05 was considered statistically significant.

Results

Assessment of Intravascular Shear Stress via Convective Heat Transfer

The sensor was deployed into NZW rabbit aortas via femoral cut-down, and navigated to the specific regions under fluoroscopic guidance (Fig. 1a and b). Real-time voltage signals were

NIH-PA Author Manuscript

NIH-PA Author Manuscript

NIH-PA Author Manuscript

measured and filtered using a Hilbert transform, from which convective heat transfer was converted to intravascular shear stress (Fig. 1c). The sensor was positioned in the aortic arch, thoracic aorta, supra renal artery, and abdominal aorta for intravascular thermal profiles (Supplementary Figure 4).

Rapid Irregular Pacing in NZW Rabbits

Surface ECG recordings were synchronized with ISS in the rabbit thoracic aorta at the baseline sinus rhythm (Fig. 2a), revealing distinct P waves, QRS complexes, and T waves. The P waves were indistinct in response to rapid irregular pacing (Fig 2b). Increasing regular pacing rate at 178.3±10.0 bpm resulted in a decrease in systolic pressure by 7.3±1.8 mmHg, a decrease in mean pressure by 3.8±1.8 mmHg, and a decrease in time-averaged shear stress by 3.8±8.4 dyne/cm^2. Rapid and irregular pacing at 178.1±38.1 bpm further decreased diastolic pressure by 9.1±4.3 mmHg, accompanied by a decrease in mean arterial pressure by 6.3±5.5 mmHg, and a similar reduction of decrease in time-averaged shear stress by 3.8±6.9 dyne/cm^2 (Table 1).

Next, we analyzed the effects of rapid irregular pacing in terms of ISS and temporal gradients ($\partial\tau/\partial t$) (Fig. 3). There were positive correlations between ISS and cycle lengths (r = 0.58), and between temporal gradients and cycle lengths (r = 0.86). There was also correlation between ISS and temporal gradients (r = 0.76). We further compared ISS with computed wall shear stress (WSS) in the thoracic aorta. ISS overlapped with computed WSS in terms of the magnitude and frequency (Fig. 3d). The minimum to maximum values of ISS ranged from 4 to 39 dyne/cm^2, which was in a close approximation to the range of computed WSS from 5 to 38 dyne/cm^2. Despite the experimental constraint to directly measure shear stress acting on the arterial wall, ISS approach provided a close approximation to the theoretical values in the thoracic aorta in an *in vivo* model. Taken together, rapid irregular pacing promoted a reduction in mean arterial pressure, ISS and $\partial\tau/\partial t$ in our *in vivo* model.

Implications of Rapid Pulse Rates on Cultured Human Aortic Endothelial Cells (HAEC)

To assess the effects of rapid pulse rates on endothelial function, we exposed HAEC to shear stress in a well-defined flow system in which we were able to vary the pulse rates at a constant time-averaged shear stress (τ_{avg}) (Supplementary Figure 3). PSS-induced eNOS mRNA up-regulation was significantly attenuated in the setting of increasing pulse rates (PSS at 50 bpm [PSS_{50}]: 1.62±0.13-fold; PSS at 100bpm [PSS_{100}]: 1.47±0.1-fold; PSS at 150 bpm [PSS_{150}]: 1.38±0.12 -fold vs. static condition, *P<0.05, n=6) (Fig. 4a); whereas OSS did not significantly alter eNOS expression. In corollary, endothelial NO production was quantified in terms of its metabolites; namely, nitrate (NO_2^-) and nitrite (NO_3^-) (Hsiai et al. 2007). We demonstrated a decrease in NO production in response to rapid pulse rates (PSS at 50 bpm [PSS_{50}]: 3.66±0.54-fold increase compared to static condition; PSS at 100bpm [PSS_{100}]: 2.45±0.12-fold; PSS at 150 bpm [PSS_{150}]: 1.87±0.47-fold, *P<0.05, n=4) (Fig. 4b). OSS further reduced NO production as reported previously (Hsiai et al. 2007) when compared to PSS condition. Hence, rapid pulse rates attenuated PSS-mediated eNOS expression and subsequent NO production.

In parallel, we assessed reactive oxygen species (ROS) production and monocytes binding. PSS is well-recognized to down-regulate $O_2^{\cdot-}$ formation (Hwang et al. 2003; Hsiai et al. 2007), whereas OSS promotes ROS production via the NADPH oxidase system (Takabe et al. 2010). Reduced pulse rates attenuated PSS-mediated reduction in DHE intensities (PSS_{50}: 26±5%, *P<0.05, n=3), whereas rapid pulse rates did not significantly alter DHE intensities (PSS_{100}: 8±5% vs. static conditions, PSS_{150}: 4±7% vs. static conditions). OSS remained a potent inducer of ROS production. Thus, rapid pulse at (PSS_{150}) reversed the salutary effect of PSS_{50} in terms of DHE-indicated ROS production (Fig. 4c).

NIH-PA Author Manuscript

NIH-PA Author Manuscript

NIH-PA Author Manuscript

We further quantified monocyte binding to HAEC. PSS_{50} attenuated monocyte binding to a greater extent compared to PSS_{150} (PSS_{50}: 37±6% reduction; PSS_{100}: 20±8%; PSS_{150}: 12±6% vs. static condition, $^{*}P<0.05$, n=4) (Fig. 4d). As a positive control (Hsiai et al. 2003), bidirectional OSS significantly increased monocyte binding (OSS: 96±40% vs. static condition, $^{\#}P<0.01$, n=4). Taken together, rapid pulse rates (P_{150}) attenuated the salutary effects of PSS_{50} in terms of eNOS mRNA expression, NO production, reduction in ROS, and monocytes binding.

Discussion

In our New Zealand White rabbit model, we elucidated how decreased cycle lengths and pulse pressure during rapid and irregular atrial pacing resulted in a reduction in both mean arterial pressure and shear stress. In our dynamic flow system, we recapitulated these in vivo findings by demonstrating how decreased cycle lengths and slew rates modulated endothelial function. Hence, both in vivo and in vitro models were complementary to provide new insights into the interplay between increased pulse rates (during sinus tachycardia or atrial fibrillation) and endothelial dysfunction.

Atrial fibrillation (AF) induces atrial and ventricular electrical remodeling (Goette et al. 1996; Xu et al. 2004). Adverse hemodynamic effects in response to rapid and irregular sequence of ventricular cycle lengths were notable for decreased cardiac output, increase pulmonary capillary wedge pressure, and increased right atrial pressure (Clark et al. 1997). AF reduced cardiac output through increased mean atrial pressure relative to left ventricular end diastolic pressure (Skinner Jr et al. 1964); thereby, decreasing stroke volume (Greenfield Jr et al. 1968; Skinner Jr et al. 1964) and cardiac output a canine model (Naito et al. 1983). Furthermore, increasing heart rates and decreasing cycle lengths reduced the Reynolds numbers, but increased the Womersley numbers (Zheng et al. 2010). In our study, deployment of flexible MEMS thermal sensors allowed for real-time measurement of convective heat transfer with high spatial and temporal resolution in the aorta of ZNW rabbits, from which we could infer a decrease in ISS and slew rates ($\partial\tau/\partial t$). Our experimental data indicated that rapid regular pacing led to a decrease in both mean blood pressure and shear stress in comparison with those of baseline measurements (Table 1). Rapid irregular pacing further reduced mean blood pressure. However, time-averaged shear stress remained similar to that of rapid regular pacing.

Experimental constraint has hampered accurate wall shear stress (WSS) measurement *in vivo*. WSS vectors were estimated from time-resolved 3-dimensional phase contrast MRI measurements of the velocity field (Papathanasopoulou et al. 2003). However, MRI is unable to detect high WSS values along the divider wall of carotid artery, and the precise measurement of velocity field near the wall and in the regions of disturbed flow remains a challenge (Pantos et al. 2007). For this reason, we have addressed how to optimize ISS measurement to approximate WSS in the region of thoracic aorta (Ai et al. 2009b). The experimental parameters that govern the deployment of the catheter-based MEMS sensors into the aorta of NZW rabbits include the dimension of coaxial wires, position of sensors in the vessel, and entrance length (L_e) to minimize flow disturbance to the sensors. In our NZW rabbit model, ISS values were influenced by the 1) presence or absence of guide wire in the aorta, 2) ratios of aorta to guide wire diameters ($n = D_{aorta}/D_{guide\ wire} = 1.5$ to 9.5), and 3) range of Reynolds numbers (116 to 1,550).

Our computational results indicated that the entrance length in response to the maximal inlet Reynolds numbers in the rabbits (Re_{max_rabbit}=459) and human abdominal aorta (Re_{max_human}=1150) were $L_{e\ rabbit}$ =1.244 cm and $L_{e\ human}$=1.985 cm, respectively. For a Womersley number greater than 1, the above L_e values could be overestimated. Sufficient

NIH-PA Author Manuscript

NIH-PA Author Manuscript

NIH-PA Author Manuscript

time was allowed for the flow to develop towards a parabolic velocity profile during individual cardiac cycles and the pulsatile flow behaved in a quasi-steady manner (Fung 1997). WSS in the presence of coaxial wire, τ_{w_wire}, can be expressed as (Ai et al. 2009b):

$$\tau_{w\_wire} = -\mu \frac{du^*}{dr}\Big|_{r=R} = E_{wss} \cdot \tau_w \quad (5)$$

where τ_w is the WSS in the absence of coaxial wire and E_{wss} is the WSS elevation factor (WEF). u denotes the velocity in the circular pipe, and R and is the radius of the pipe.

$$E_{wss} = \frac{n^2 (2n^2 \ln n - n^2 + 1)}{2[(n^4 - 1)\ln n - (n^2 - 1)^2]} \quad (6)$$

Similarly, the shear stress on the MEMS sensor, τ_{i_wire}, can be evaluated at $r = R_i$ (radius of the catheter/coaxial wire):

$$\tau_{i\_wire} = -\mu \frac{dU}{dr}\Big|_{r=R_i} = E_{iss} \cdot \tau_w \quad (7)$$

where E_{iss} is defined as the ISS elevation factor (IEF):

$$E_{iss} = \frac{n^3 (2\ln n - n^2 + 1)}{2[(n^4 - 1)\ln n - (n^2 - 1)^2]} \quad (8)$$

To optimize real-time ISS in NZW rabbit, CFD analyses revealed that an entrance length of 2.9 mm and the diameter ratio (n) of 4.5 would minimize the pressure and shear stress elevation in the rabbit aorta. When the catheter was positioned off the center of vessel, Velusamy and Garg (Velusamy and Garg 1994) reported that an eccentricity of the velocity profiles developed, and shear stress on the catheter and the vessel wall varied circumferentially (Ai et al. 2009a). In humans, the diameter ratio could approach to 100 for an aortic inner diameter of 2.5 cm with a catheter outer diameter of 0.254 mm. Hence, ISS assessment could be further optimized by positioning the catheter near the vessel wall using a steerable catheter with a large diameter ratio in a large animal model (Ai et al. 2009b). In NZW rabbits, convective heat transfer-inferred time-averaged ISS was within the range of computed WSS by 18.5% in the presence of guide wire (Ai et al. 2009b; Ai et al. 2010). Thus, the application of ISS afforded a reasonable approximation to computed WSS in the thoracic aorta.

Increasing evidence has supported a link between chronic AF and vascular endothelial dysfunction (Yoshino et al. 2011). Patients with AF have been reported to harbor elevated circulating Von Willebrand factor (vWF) and increased E-selectin (Freestone et al. 2008; Tveit et al. 2007). AF is also implicated in decrease in endothelial dependent vasodilation in forearm vessels (Freestone et al. 2008; Guazzi et al. 2007), serum nitrates (Minamino et al. 1997; Nikitovic et al. 2002), and coronary flow reserve (CFR) (Skalidis et al. 2008). Our *in vitro* flow system allows for delivering a constant time-averaged shear stress (τ_{avg}) while varying pulse rates to recapitulate rapid pacing-mediated reduction in temporal gradients ($\partial\tau/\partial t$) and pulse pressure (∂P) in rabbits. Our current study demonstrated that rapid pulse rates modulated endothelial NO and ROS production and interaction with monocytes binding; thus, supporting the rapid and irregular pacing model to further elucidate the molecular mechanisms underlying AF-mediated endothelial dysfunction in an *in vitro* flow system.

NIH-PA Author Manuscript

NIH-PA Author Manuscript

NIH-PA Author Manuscript

Mounting evidence supports that fluid shear stress is intimately involved in vascular oxidative stress (Madamanchi et al. 2005), inflammatory responses, and atherosclerosis (Davies et al. 1986; Topper et al. 1996; Nerem et al. 1998; Berk 2008). In the medial wall of arterial bifurcations or relatively straight segments of carotid arteries, unidirectional pulsatile flow (net positive forward flow) develops, whereas in the lateral wall or atheroprone regions, flow separation and secondary flow develop. In response to cardiac contraction, the migrating stagnation points generate low and oscillating flow (bidirectional zero net forward flow), otherwise known as disturbed or secondary flow (Fung 1997). Pulsatile flow down-regulates adhesion molecules and reactive oxygen species, whereas oscillatory flow increases oxidative stress, promoting the initiation of atherosclerosis (De Keulenaer et al. 1998; Landmesser and Harrison 2001; Sorescu et al. 2002; Witztum 1994; Ziegler et al. 1998). PSS attenuates vascular $O_2^{\cdot -}$ production, in part, via down-regulation of NADPH oxidase system (Hwang et al. 2003). In the present study, we found that pulse rates ranging from 50 bpm to 150 bpm influenced eNOS mRNA expression and subsequent NO production. While the precise molecular mechanisms remain to be defined, we provided a flow model system to isolate the effects of rapid pulse rates on endothelial responses with clinical relevance

Analysis of sensor performance in terms of temperature overheat ratio and thermal coefficient of resistance further supported feasibility of flexible MEMS sensors for real-time physiological recording with high sensitivity and frequency responses. We previously reported changes in heat transfer in atherosclerotic lesions in fat-fed NZW rabbits (Yu et al. 2011). Here, we further assessed rapid and irregular pacing-mediated changes in heat transfer-inferred ISS and $\partial\tau/\partial t$. Changes in temporal gradient or known as slew rates ($\partial\tau/\partial t$) in shear stress have been well-recognized in nitric oxide-dependent dilation of arterioles, endothelial cell proliferation, and monocytes-adhesion to active lipid-induced endothelial cells (Bagi et al. 2005; White et al. 2001; Hsiai et al. 2002; Hsiai et al. 2001). Thus, heat transfer-inferred ISS and $\partial\tau/\partial t$ offered a potential entry point to link rapid and irregular pulse rates with vascular endothelial function.

In conclusion, the current study provides an *in vivo* model to link AF-mediated changes in convective heat transfer with a decrease in ISS in a NZW rabbit model. We established a link between rapid pulse rates and endothelial responses in a well-defined flow system. Our intravascular heat transfer strategy ($\partial\tau$, $\partial\tau/\partial t$, and ∂P) will likely provide a basis to further investigate whether AF cardioversion to sinus rhythm improves endothelial function (Yoshino et al. 2011).

Supplementary Material

Refer to Web version on PubMed Central for supplementary material.

Acknowledgments

We would like to thank Sharon Hale, Wangde Dai and Dr. Robert Kloner at Good Samaritan Hospital for housing the rabbits and performing the animal surgeries. We also like to thank Rosalinda Wenby and Dr. Herbert Meiselman for assisting with rabbit blood viscosity and hematocrit measurements. This project was supported by NHLBI 091302 (TKH) and NHLB 083015 (TKH).

References

Ai L, Yu H, Dai W, Hale SL, Kloner RA, Hsiai TK. Real-time intravascular shear stress in the rabbit abdominal aorta. Biomedical Engineering, IEEE Transactions on. 2009a; 56 (6):1755–1764.

NIH-PA Author Manuscript

NIH-PA Author Manuscript

NIH-PA Author Manuscript

Ai L, Yu H, Takabe W, Paraboschi A, Yu F, Kim E, Li R, Hsiai TK. Optimization of intravascular shear stress assessment in vivo. Journal of biomechanics. 2009b; 42 (10):1429–1437. [PubMed: 19457490]

Ai L, Zhang L, Dai W, Hu C, Kirk Shung K, Hsiai TK. Real-time assessment of flow reversal in an eccentric arterial stenotic model. Journal of biomechanics. 2010

Bagi Z, Frangos JA, Yeh JC, White CR, Kaley G, Koller A. PECAM-1 mediates NO-dependent dilation of arterioles to high temporal gradients of shear stress. Arteriosclerosis, thrombosis, and vascular biology. 2005; 25 (8):1590–1595.

Berk BC. Atheroprotective signaling mechanisms activated by steady laminar flow in endothelial cells. Circulation. 2008; 117 (8):1082. [PubMed: 18299513]

Clark M, David M, Plumb M, Vance J, Epstein M, Andrew E, Kay M. Hemodynamic effects of an irregular sequence of ventricular cycle lengths during atrial fibrillation. Journal of the American College of Cardiology. 1997; 30 (4):1039–1045. [PubMed: 9316536]

Davies PF, Remuzzi A, Gordon EJ, Dewey CF, Gimbrone MA. Turbulent fluid shear stress induces vascular endothelial cell turnover in vitro. Proceedings of the National Academy of Sciences of the United States of America. 1986; 83 (7):2114. [PubMed: 3457378]

De Keulenaer GW, Chappell DC, Ishizaka N, Nerem RM, Alexander RW, Griendling KK. Oscillatory and steady laminar shear stress differentially affect human endothelial redox state: role of a superoxide-producing NADH oxidase. Circulation research. 1998; 82 (10):1094. [PubMed: 9622162]

Deedwania PC, Lardizabal JA. Atrial fibrillation in heart failure: a comprehensive review. The American journal of medicine. 2010; 123 (3):198–204. [PubMed: 20193823]

Ehrlich JR, Kaluzny M, Baumann S, Lehmann R, Hohnloser SH. Biomarkers of structural remodelling and endothelial dysfunction for prediction of cardiovascular events or death in patients with atrial fibrillation. Clinical Research in Cardiology. 2011:1–8.

Freestone B, Chong AY, Nuttall S, Lip GYH. Impaired flow mediated dilatation as evidence of endothelial dysfunction in chronic atrial fibrillation::: Relationship to plasma von Willebrand factor and soluble E-selectin levels. Thrombosis research. 2008; 122 (1):85–90. [PubMed: 17996280]

Fung, Y. Biomechanics: circulation. Springer Verlag; 1997.

Fuster V, Ryden LE, Cannom DS, Crijns HJ, Curtis AB, Ellenbogen KA, Halperin JL, Le Heuzey JY, Kay GN, Lowe JE. ACC/AHA/ESC 2006 guidelines for the management of patients with atrial fibrillation: a report of the American College of Cardiology/American Heart Association Task Force on practice guidelines and the European Society of Cardiology Committee for practice guidelines (Writing committee to revise the 2001 guidelines for the management of patients with atrial fibrillation): developed in collaboration with the European Heart Rhythm Association and the Heart Rhythm Society. Circulation. 2006; 114 (7):e257. [PubMed: 16908781]

Go AS, Hylek EM, Phillips KA, Chang YC, Henault LE, Selby JV, Singer DE. Prevalence of diagnosed atrial fibrillation in adults. JAMA: the journal of the American Medical Association. 2001; 285 (18):2370–2375. [PubMed: 11343485]

Goette A, Hammwöhner M, Bukowska A, Scalera F, Martens-Lobenhoffer J, Dobrev D, Ravens U, Weinert S, Medunjanin S, Lendeckel U. The impact of rapid atrial pacing on ADMA and endothelial NOS. International Journal of Cardiology. 2012; 154 (2):141–146. [PubMed: 20926145]

Goette A, Honeycutt C, Langberg JJ. Electrical remodeling in atrial fibrillation: time course and mechanisms. Circulation. 1996; 94 (11):2968–2974. [PubMed: 8941128]

Greenfield JC Jr, Harley A, Thompson HK, Wallace AG. Pressure-flow studies in man during atrial fibrillation. Journal of Clinical Investigation. 1968; 47 (10):2411–2421. [PubMed: 5676530]

Guazzi M, Arena R. Endothelial dysfunction and pathophysiological correlates in atrial fibrillation. Heart. 2009; 95 (2):102–106. [PubMed: 19109515]

Guazzi M, Belletti S, Lenatti L, Bianco E, Guazzi M. Effects of cardioversion of atrial fibrillation on endothelial function in hypertension or diabetes. European journal of clinical investigation. 2007; 37 (1):26–34. [PubMed: 17181564]

NIH-PA Author Manuscript

NIH-PA Author Manuscript

NIH-PA Author Manuscript

Haissaguerre M, Jaïs P, Shah DC, Takahashi A, Hocini M, Quiniou G, Garrigue S, Le Mouroux A, Le Métayer P, Clémenty J. Spontaneous initiation of atrial fibrillation by ectopic beats originating in the pulmonary veins. New England Journal of Medicine. 1998; 339 (10):659–666. [PubMed: 9725923]

Hsiai TK, Cho SK, Honda HM, Hama S, Navab M, Demer LL, Ho CM. Endothelial Cell Dynamics under Pulsating Flows: Significance of High Versus Low Shear Stress Slew Rates ($\partial\tau/\partial\tau$). Annals of biomedical engineering. 2002; 30 (5):646–656. [PubMed: 12108839]

Hsiai TK, Cho SK, Reddy S, Hama S, Navab M, Demer LL, Honda HM, Ho CM. Pulsatile flow regulates monocyte adhesion to oxidized lipid-induced endothelial cells. Arteriosclerosis, thrombosis, and vascular biology. 2001; 21 (11):1770–1776.

Hsiai TK, Cho SK, Wong PAKK, Ing M, Salazar A, Sevanian A, Navab M, Demer LL, Ho CM. Monocyte recruitment to endothelial cells in response to oscillatory shear stress. The FASEB journal. 2003; 17 (12):1648.

Hsiai TK, Cho SK, Wong PK, Ing MH, Salazar A, Hama S, Navab M, Demer LL, Ho CM. Micro sensors: linking real-time oscillatory shear stress with vascular inflammatory responses. Annals of Biomedical Engineering. 2004; 32 (2):189–201. [PubMed: 15008367]

Hsiai TK, Hwang J, Barr ML, Correa A, Hamilton R, Alavi M, Rouhanizadeh M, Cadenas E, Hazen SL. Hemodynamics influences vascular peroxynitrite formation: Implication for low-density lipoprotein apo-B-100 nitration. Free Radical Biology and Medicine. 2007; 42 (4):519–529. [PubMed: 17275684]

Hwang J, Michael H, Salazar A, Lassegue B, Griendling K, Navab M, Sevanian A, Hsiai TK. Pulsatile Versus Oscillatory Shear Stress Regulates NADPH Oxidase Subunit Expression. Circulation research. 2003; 93 (12):1225–1232. [PubMed: 14593003]

Hwang J, Rouhanizadeh M, Hamilton RT, Lin TC, Eiserich JP, Hodis HN, Hsiai TK. 17 [beta]-Estradiol reverses shear-stress-mediated low density lipoprotein modifications. Free Radical Biology and Medicine. 2006; 41 (4):568–578. [PubMed: 16863990]

Kern, MJ.; Lim, MJ.; Goldstein, JA. Hemodynamic rounds: interpretation of cardiac pathophysiology from pressure waveform analysis. Wiley-Blackwell; 2009.

Landmesser U, Harrison DG. Oxidant stress as a marker for cardiovascular events: Ox marks the spot. Circulation. 2001; 104 (22):2638. [PubMed: 11723010]

Li YSJ, Haga JH, Chien S. Molecular basis of the effects of shear stress on vascular endothelial cells. Journal of biomechanics. 2005; 38 (10):1949–1971. [PubMed: 16084198]

Madamanchi NR, Vendrov A, Runge MS. Oxidative stress and vascular disease. Arteriosclerosis, thrombosis, and vascular biology. 2005; 25 (1):29.

Matsue Y, Suzuki M, Abe M, Ono M, Seya M, Nakamura T, Iwatuka R, Mizukami A, Toyama K, Kumasaka L. Endothelial Dysfunction in Paroxysmal Atrial Fibrillation as a Prothrombotic State: Comparison with Permanent/Persistent Atrial Fibrillation. Journal of atherosclerosis and thrombosis. 2011; 18 (4):298–304. [PubMed: 21224522]

Minamino T, Kitakaze M, Sato H, Asanuma H, Funaya H, Koretsune Y, Hori M. Plasma levels of nitrite/nitrate and platelet cGMP levels are decreased in patients with atrial fibrillation. Arteriosclerosis, thrombosis, and vascular biology. 1997; 17 (11):3191–3195.

Naito M, David D, Michelson Eric L, Schaffenburg M, Dreifus LS. The hemodynamic consequences of cardiac arrhythmias: evaluation of the relative roles of abnormal atrioventricular sequencing, irregularity of ventricular rhythm and atrial fibrillation in a canine model. American heart journal. 1983; 106 (2):284–291. [PubMed: 6869209]

Nattel S. New ideas about atrial fibrillation 50 years on. Nature. 2002; 415 (6868):219–226. [PubMed: 11805846]

Nattel S. Dronedarone in Atrial Fibrillation—Jekyll and Hyde? New England Journal of Medicine. 2011; 365 (24):2321–2322. [PubMed: 22082122]

Nerem RM, Alexander RW, Chappell DC, Medford RM, Varner SE, TAYLOR WR. The study of the influence of flow on vascular endothelial biology. The American journal of the medical sciences. 1998; 316 (3):169. [PubMed: 9749558]

Nikitovic D, Zacharis EA, Manios EG, Malliaraki NE, Kanoupakis EM, Sfiridaki KI, Skalidis EI, Margioris AN, Vardas PE. Plasma levels of nitrites/nitrates in patients with chronic atrial

NIH-PA Author Manuscript

NIH-PA Author Manuscript

NIH-PA Author Manuscript

fibrillation are increased after electrical restoration of sinus rhythm. Journal of interventional cardiac electrophysiology. 2002; 7 (2):171–176. [PubMed: 12397227]

Pantos I, Patatoukas G, Efstathopoulos EP, Katritsis D. In vivo wall shear stress measurements using phase-contrast MRI. Expert review of cardiovascular therapy. 2007; 5 (5):927–938. [PubMed: 17867922]

Papafaklis MI, Koskinas KC, Chatzizisis YS, Stone PH, Feldman CL. In-vivo assessment of the natural history of coronary atherosclerosis: vascular remodeling and endothelial shear stress determine the complexity of atherosclerotic disease progression. Current Opinion in Cardiology. 2010; 25 (6):627–638. [PubMed: 20838338]

Papathanasopoulou P, Zhao S, Köhler U, Robertson MB, Long Q, Hoskins P, Yun Xu X, Marshall I. MRI measurement of time-resolved wall shear stress vectors in a carotid bifurcation model, and comparison with CFD predictions. Journal of Magnetic Resonance Imaging. 2003; 17 (2):153–162. [PubMed: 12541221]

Pietraforte D, Salzano AM, Scorza G, Minetti M. Scavenging of reactive nitrogen species by oxygenated hemoglobin: globin radicals and nitrotyrosines distinguish nitrite from nitric oxide reaction. Free Radical Biology and Medicine. 2004; 37 (8):1244–1255. [PubMed: 15451064]

Raviele A, Ronco F. Endothelial Dysfunction and Atrial Fibrillation: What is the Relationship? Journal of Cardiovascular Electrophysiology. 2010; 22 (4):376–382. [PubMed: 20958832]

Skalidis EI, Hamilos MI, Karalis IK, Chlouverakis G, Kochiadakis GE, Vardas PE. Isolated atrial microvascular dysfunction in patients with lone recurrent atrial fibrillation. Journal of the American College of Cardiology. 2008; 51 (21):2053–2057. [PubMed: 18498961]

Skinner NS Jr, Mitchell JH, Wallace AG, Sarnoff SJ. Hemodynamic consequences of atrial fibrillation at constant ventricular rates. The American Journal of Medicine. 1964; 36 (3):342–350. [PubMed: 14131878]

Sorescu D, Weiss D, Lassegue B, Clempus RE, Szocs K, Sorescu GP, Valppu L, Quinn MT, Lambeth JD, Vega JD. Superoxide production and expression of nox family proteins in human atherosclerosis. Circulation. 2002; 105 (12):1429. [PubMed: 11914250]

Sun P, Zhang Y, Yu F, Parks E, Lyman A, Wu Q, Ai L, Hu CH, Zhou Q, Shung K. Micro-electrocardiograms to study post-ventricular amputation of zebrafish heart. Annals of biomedical engineering. 2009; 37 (5):890–901. [PubMed: 19280341]

Takabe W, Jen N, Ai L, Hamilton R, Wang S, Holmes K, Darbandi F, Khalsa B, Bressler S, Barr M. Oscillatory Shear Stress Induces Mitochondrial Superoxide Production: Implication of NADPH Oxidase and c-Jun NH 2-terminal Kinase Signaling. Antioxidants & Redox Signaling (ja). 2010

Topper JN, Cai J, Falb D, Gimbrone MA. Identification of vascular endothelial genes differentially responsive to fluid mechanical stimuli: cyclooxygenase-2, manganese superoxide dismutase, and endothelial cell nitric oxide synthase are selectively up-regulated by steady laminar shear stress. Proceedings of the National Academy of Sciences of the United States of America. 1996; 93 (19): 10417. [PubMed: 8816815]

Tveit A, Seljeflot I, Grundvold I, Abdelnoor M, Smith P, Arnesen H. Effect of candesartan and various inflammatory markers on maintenance of sinus rhythm after electrical cardioversion for atrial fibrillation. The American journal of cardiology. 2007; 99 (11):1544–1548. [PubMed: 17531578]

Velusamy K, Garg VK. Entrance Flow in Eccentric Annular Ducts. International Journal for Numerical Methods in Fluids. 1994; 19 (6):493–512.

Wann LS, Curtis AB, Ellenbogen KA, Estes N III, Ezekowitz MD, Jackman WM, January CT, Lowe JE, Page RL, Slotwiner DJ. 2011 ACCF/AHA/HRS Focused Update on the Management of Patients with Atrial Fibrillation (Update on Dabigatran): A Report of the American College of Cardiology Foundation/American Heart Association Task Force on Practice Guidelines. Circulation. 2011 CIR. 0b013e31820f31814c31820v31821.

White CR, Haidekker M, Bao X, Frangos JA. Temporal gradients in shear, but not spatial gradients, stimulate endothelial cell proliferation. Circulation. 2001; 103 (20):2508–2513. [PubMed: 11369693]

Witztum J. The oxidation hypothesis of atherosclerosis. Lancet. 1994; 344 (8925):793–795. [PubMed: 7916078]

NIH-PA Author Manuscript

NIH-PA Author Manuscript

NIH-PA Author Manuscript

Xu J, Cui G, Esmailian F, Plunkett M, Marelli D, Ardehali A, Odim J, Laks H, Sen L. Atrial extracellular matrix remodeling and the maintenance of atrial fibrillation. Circulation. 2004; 109 (3):363–368. [PubMed: 14732752]

Yoshino S, Yoshikawa A, Hamasaki S, Ishida S, Oketani N, Saihara K, Okui H, Ichiki H, Kuwahata S, Fujita S. Chronic atrial fibrillation impairs endothelial function that improves after sinus rhythm restoration by catheter ablation. Journal of the American College of Cardiology. 2011; 57 (14 Suppl S):E1428.

Yu F, Ai L, Dai W, Rozengurt N, Yu H, Hsiai TK. MEMS Thermal Sensors to Detect Changes in Heat Transfer in the Pre-Atherosclerotic Regions of Fat-Fed New Zealand White Rabbits. Annals of biomedical engineering. 2011:1–9.

Yu F, Huang J, Adlerz K, Jadvar H, Hamdan MH, Chi N, Chen JN, Hsiai TK. Evolving Cardiac Conduction Phenotypes in Developing Zebrafish Larvae: Implications to Drug Sensitivity. Zebrafish. 2010; 7 (4):325–331. [PubMed: 20958244]

Yu H, Ai L, Rouhanizadeh M, Patel D, Kim ES, Hsiai TK. Flexible polymer sensors for in vivo intravascular shear stress analysis. Microelectromechanical Systems, Journal of. 2008; 17 (5): 1178–1186.

Zheng H, Huo Y, Svendsen M, Kassab GS. Effect of blood pressure on vascular hemodynamics in acute tachycardia. Journal of Applied Physiology. 2010; 109 (6):1619–1627. [PubMed: 20884836]

Ziegler T, Bouzourene K, Harrison VJ, Brunner HR, Hayoz D. Influence of oscillatory and unidirectional flow environments on the expression of endothelin and nitric oxide synthase in cultured endothelial cells. Arteriosclerosis, thrombosis, and vascular biology. 1998; 18 (5):686.

Zipes D, Camm A, Borggrefe M, Buxton A, Chaitman B, Fromer M, Gregoratos G, Klein G, Moss A, Myerburg R. American College of Cardiology/American Heart Association Task Force; European Society of Cardiology Committee for Practice Guidelines; European Heart Rhythm Association; Heart Rhythm Society. ACC/AHA/ESC 2006 Guidelines for Management of Patients With Ventricular Arrhythmias and the Prevention of Sudden Cardiac Death: A report of the American College of Cardiology/American Heart Association Task Force and the European Society of Cardiology Committee for Practice Guidelines (writing committee to develop Guidelines for Management of Patients With Ventricular Arrhythmias and the Prevention of Sudden Cardiac Death): Developed in collaboration with the European Heart Rhythm Association and the Heart Rhythm Society. Circulation. 2006; 114 (10):385–484.

NIH-PA Author Manuscript
NIH-PA Author Manuscript
NIH-PA Author Manuscript

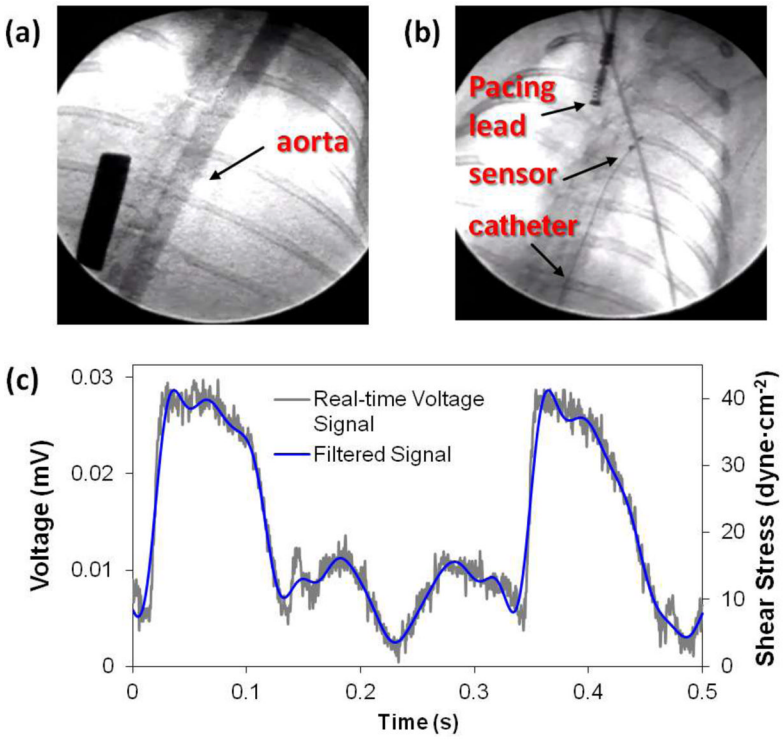

Figure 1. Assessment of intravascular shear stress via convective heat transfer

(a) Rabbit aorta was visualized by fluoroscopic angiography with contrast for measurements of aortic diameter. **(b)** Fluoroscopy further guided deployment of flexible intravascular sensor to the ascending aorta and the pacing lead to the right atrium. **(c)** Real-time intravascular measurements **(grey line)** captured the pulsatile voltage profiles. The signal was filtered by Hilbert wavelet transform **(blue line)**. Voltage measurements were then converted to the corresponding shear stress values as described in the methods.

NIH-PA Author Manuscript

NIH-PA Author Manuscript

NIH-PA Author Manuscript

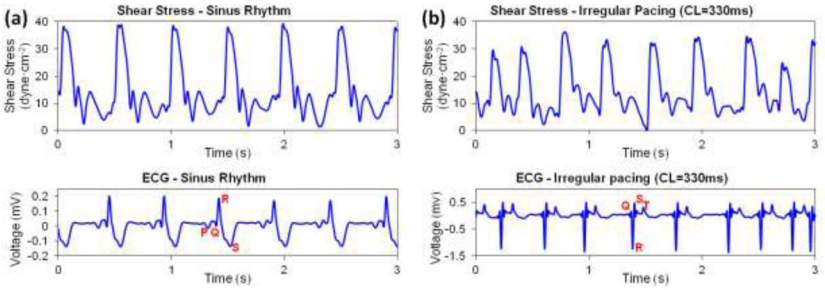

Figure 2. Intravascular shear stress in synchrony with surface ECG recording

(a) ISS and surface ECG were synchronized in the setting of normal sinus rhythm. **(b)** Atrial pacing at an irregular rhythm resulted in indistinct P waves and irregular R-R intervals, as well as negative QRS amplitude in response to atrial pacing.

NIH-PA Author Manuscript

NIH-PA Author Manuscript

NIH-PA Author Manuscript

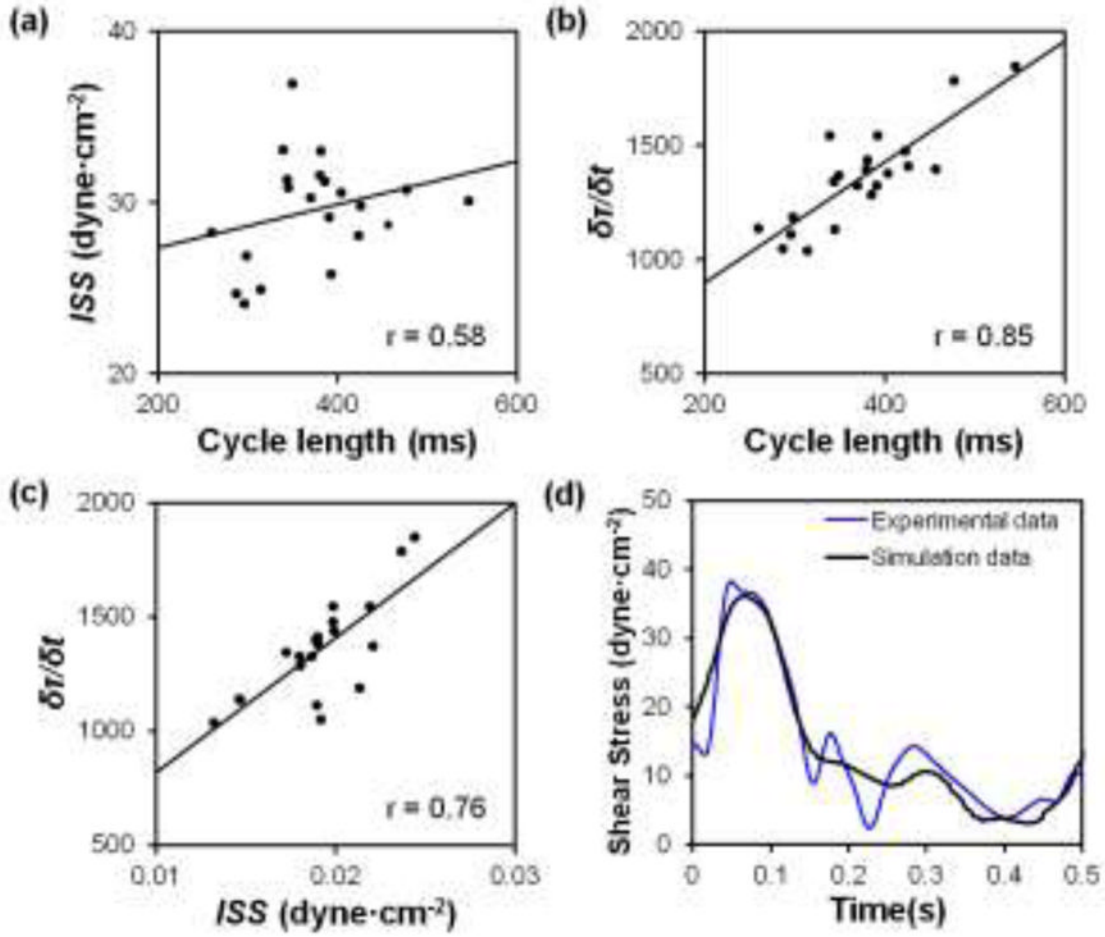

Figure 3. Rapid and irregular pacing altered ISS and temporal gradients

We analyzed the relation between changes in intravascular shear stresses (ISS) and cycle lengths, between temporal gradients ($\partial\tau/\partial t$) and cycle lengths, and between slew rates and shear stress in response to irregular and tachycardia pacing protocol. **(a)** Changes in shear stress correlated with the cycle lengths (r = 0.58). **(b)** Changes in $\partial\tau/\partial t$ also correlated with the cycle lengths (r = 0.86). **(c)** Changes in $\partial\tau/\partial t$ further correlated with changes in ISS (r = 0.76). **(d)** Experimental ISS and simulated wall shear stress (WSS) overlapped in terms of magnitude and frequency in a resting rabbit. ISS ranged between 4 to 39 dyne/cm^2, corresponding to a simulated range of 5 to 38 dyne/cm^2.

NIH-PA Author Manuscript
NIH-PA Author Manuscript
NIH-PA Author Manuscript

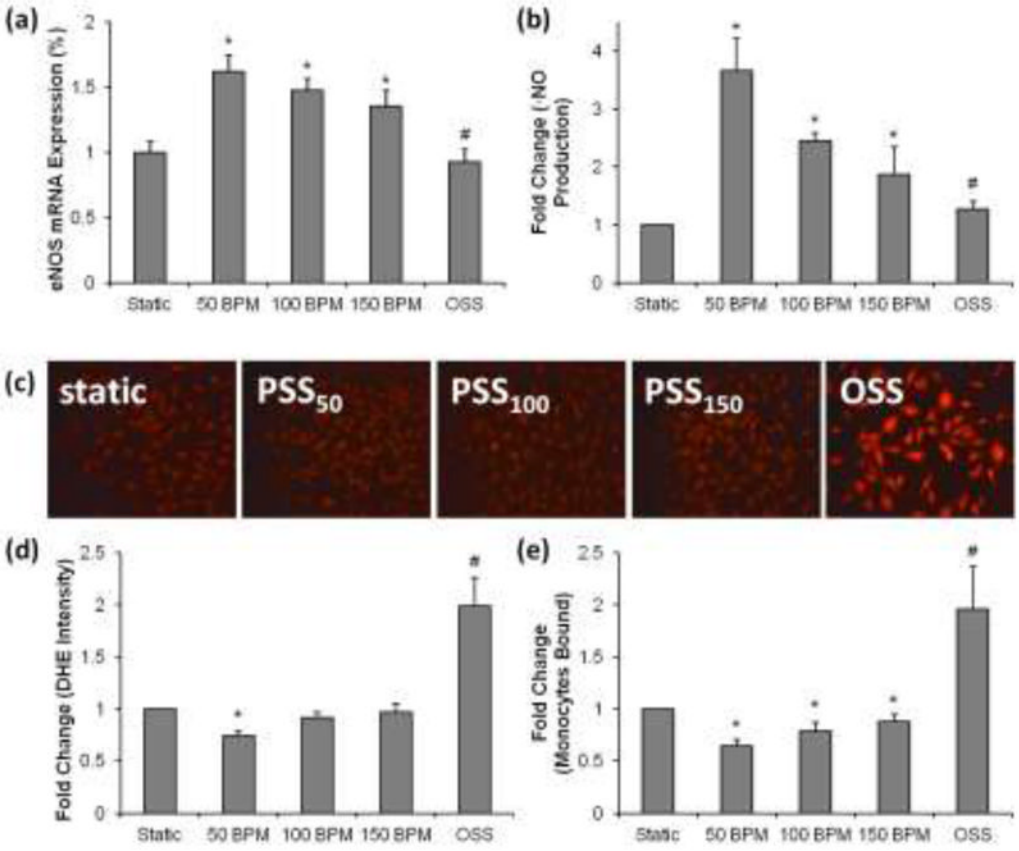

Figure 4. Rapid pulse rates modulated endothelial responses

(a) Decreases in eNOS mRNA expression in response to increases in pulse rates. At an identical time-averaged shear stress (τ_{ave}), eNOS mRNA expression in HAECs was significantly up-regulated by 1.62±0.13-fold in response to PSS at 50 BPM (PSS_{50}) and by 1.38±0.12-fold in response to PSS at 150 bpm (PSS_{150}) (*P<0.05 vs. static condition, n=6). eNOS mRNA expression remained unchanged statistically in response to oscillatory shear stress at 60 bpm (#P>0.05 vs. static condition, n=6). **(b) Decreases in NO metabolites production in response to increases in pulse rates.** NO metabolites, nitrate (NO_2^-) and nitrite (NO_3^-), were increased by 3.66±0.54-fold in response to PSS_{50} and by 1.87±0.47-fold in response to PSS_{150} (*P<0.05 vs. static condition, n=4). OSS metabolite production in response to OSS was also elevated (#P<0.05 vs. static condition, n=6). **(c, d) The effects of pulsatile and oscillatory shear stress on DHE intensities.** Dihydroethidium fluorescent intensities. PSS_{50} significantly decreased fluorescent intensities as indicated by DHE staining in HAEC (*P<0.05, n=3), whereas OSS significantly increased DHE intensities (#P<0.05, n=3). PSS100 and PSS150 did not significantly reduce DHE intensities. DHE intensities were quantified from fluorescent images in the graph. **(e) Incremental monocyte binding in response to increases in pulse rates.** PSS at 50 BPM (PSS_{50}) attenuated monocyte binding by 37±6%, whereas PSS at 150 bpm (PSS_{150}) attenuated monocyte binding by 12±6% (*P<0.05 vs. static condition, n=4). OSS at 60 bpm significantly increased monocyte binding by 96% (#P<0.01 vs. static condition, n=4).

NIH-PA Author Manuscript

NIH-PA Author Manuscript

NIH-PA Author Manuscript

Table 1

Changes in arterial pressure in response to atrial pacing

Systolic, diastolic, mean arterial blood pressure, and time-averaged shear stress in response to baseline sinus rhythm at 122.1±5.4, regular and tachycardia atrial pacing at 178.3±10.0, and irregular pacing at 178.1±38.1. Increasing atrial pacing rates resulted in a reduction in systolic, diastolic, mean blood pressures, and time-averaged shear stress. Irregular pacing led to a further reduction in blood pressures, while time-averaged shear stress remained similar

	Baseline Rhythm	Regular Cardiac Pacing	Irregular Cardiac Pacing
Heart Rate (bpm)	122.1 ± 5.4	178.3 ± 10.0	178.1 ± 38.1
Systolic Pressure (mmHg)	99.4 ± 0.9	92.1 ± 1.6	90.3 ± 4.2
Diastolic Pressure (mmHg)	74.9 ± 1.2	73.2 ± 1.9	68.4 ± 5.3
Mean Pressure(mmHg)	83.0 ± 1.0	79.1 ± 1.5	75.9 ± 3.6
Time Averaged Shear Stress (dyne·cm^{-2})	28.6 ± 6.2	24.8 ± 5.7	24.8 ± 3.0